Magnetic structure of the zigzag chain family $Na_xCa_{1-x}V_2O_4$ determined by muon-spin rotation

Oren Ofer,[1,*] Yutaka Ikedo,[2,†] Tatsuo Goko,[1] Martin Månsson,[3] Jun Sugiyama,[2] Eduardo J. Ansaldo,[1] Jess H. Brewer,[1,4] Kim H. Chow,[5] and Hiroya Sakurai[6]

[1]*TRIUMF, 4004 Wesbrook Mall, Vancouver, British Columbia, Canada V6T 2A3*

[2]*Toyota Central Research and Development Laboratories Inc., Nagakute, Aichi 480-1192, Japan*

[3]*Laboratory for Neutron Scattering, Paul Scherrer Institute, ETH Zürich, CH-5232 Villigen PSI, Switzerland*

[4]*Department of Physics and Astronomy, University of British Columbia, Vancouver, British Columbia, Canada V6T 2A3*

[5]*Department of Physics, University of Alberta, Edmonton, Alberta, Canada T6G 2G7*

[6]*National Institute for Materials Science, Namiki, Tsukuba, Ibaraki 305-0044, Japan*

(Received 17 June 2010; published 7 September 2010)

We present muon-spin-rotation measurements on polycrystalline samples of the complete family of the antiferromagnetic (AF) *zigzag* chain compounds, $Na_xCa_{1-x}V_2O_4$. In this family, we explore the magnetic properties from the metallic NaV_2O_4 to the insulating CaV_2O_4. We find a critical $x_c(\sim 0.833)$ which separates the low and high Na-concentration-dependent transition temperature and its magnetic ground state. In the $x<x_c$ compounds, the magnetic ordered phase is characterized by a single homogenous phase and the formation of incommensurate spin-density-wave order. Whereas in the $x>x_c$ compounds, multiple subphases appear with temperature and x. Based on the muon data obtained in zero external magnetic field, a careful dipolar field simulation was able to reproduce the muon behavior and indicates a modulated helical incommensurate spin structure of the metallic AF phase. The incommensurate modulation period obtained by the simulation agrees with that determined by neutron diffraction.

DOI: 10.1103/PhysRevB.82.094410 PACS number(s): 76.75.+i, 75.50.Lk, 75.50.Ee

I. INTRODUCTION

Experimental and theoretical studies of quasi-one-dimensional (quasi-1D) magnets have flourished recently. On theoretical grounds, such systems seem to experience low dimensionality combined with frustrated interactions of nearest-neighbors and next-nearest-neighbors competition, leading to spin-density waves (SDWs) forming chiral order[1] and other exotic ground states.[2,3] Experimentally, progress has accelerated due to recent use of high-pressure techniques,[4–6] enabling synthesis of numerous compounds. Such materials show remarkable physical behavior,[7–9] where the nature behind these phenomena is governed by a strong spin-spin interaction along one direction combined with a much weaker interaction in the other directions. A novel quasi-1D spin system of particular interest is NaV_2O_4 (NVO),[10] which is isostructural with CaV_2O_4 (CVO).[11] Unlike other vanadate compounds, which are spinels,[12] NVO and CVO posses an orthorhombic structure with the *Pnma* space group, where irregular hexagonal 1D channels are formed by a series of edge-sharing VO_6 octahedra aligned along the b axis. The magnetic V ions are thus arranged in a 1D *zigzag* chain. Despite their closely related chemical and crystallographical nature, they exhibit dramatically different magnetic and electronic properties. The metallic NVO incorporates a mixed valence $V^{+3.5}$ state and undergoes an antiferromagnetic (AF) transition at $T_N=140$ K, with a complex magnetic ground state.[10,13] In fact, recent neutron studies indicate the formation of incommensurate (IC) magnetic order in NVO below T_N.[14] The insulating CVO, on the other hand, has a V^{+3} valence $(t_{2g}^2, S=1)$ with an AF transition at $T_N=70$ K, coexisting with intrachain ferromagnetic interactions. Furthermore, the chemical substitution of Na for Ca causes an interesting insulator to metal transition at a critical Na concentration $x>x_c\sim 0.83$ in $Na_xCa_{1-x}V_2O_4$ (NCVO). The presence of the insulator-to-metal transition suggests a dynamic change in the electronic structure of NCVO with x, resulting in the change in its magnetic ground state. It is therefore desirable to systematically investigate the evolution of the microscopic magnetic order/disorder in NCVO.

Recently, through the use of positive muon-spin rotation and relaxation (μ^+SR), we found the formation of static AF order for a few NCVO compounds below their T_N and proposed a magnetic phase diagram.[13] μ^+SR is known to be a powerful technique for studies on microscopic magnetic nature in solids, due to its inherent 100% spin polarization and local sensitivity. The most interesting feature in NCVO is the unusual coexistence of AF order and metallic behavior below T_N for NCVO with $x>x_{cr}$. The main purpose of this paper is, therefore, to clarify the microscopic magnetic ground state of the entire NCVO family through the use of μ^+SR and numerical simulations based on dipolar field calculations. This is, to our knowledge, a pioneering attempt to deduce the incommensurate modulation period *from* μ^+SR data. We also seek to complete the magnetic phase diagram of NCVO by additional μ^+SR measurements on insulating and metallic NCVO samples with $x=0.166$, 0.41, 0.875, and 0.958, which were not described in our previous report. Our results reveal that the magnetic ground state in the insulating compounds with $0<x\leq x_c$ are also an incommensurate magnetically ordered phase. This means that not only pure CaV_2O_4 but also the complete family of NCVO exhibit incommensurate magnetic order at low T, concurrent with the change in the valence state of the V ion from 3 to 3.5 with increasing x. This could provide a very interesting challenge for theorists: to predict the magnetic phase diagram of this zigzag chain compounds.

II. EXPERIMENT

Polycrystalline samples of NCVO were prepared by a solid-state reaction technique under a pressure of 6 GPa using CaV_2O_4, $Na_4V_2O_7$, and V_2O_3 powders as starting materials. A mixture of the three powders was packed in an Au capsule, then heated at 1300 °C for 1 h, and finally quenched to ambient T. A powder x-ray diffraction analysis showed that all the samples were almost single phase with an orthorhombic system, *Pnma* space group, at ambient T. dc-χ measurements showed that all our samples have almost the same T dependence as that in the previous report.[15] The preparation and characterization of the samples have been reported in greater detail elsewhere.[15]

The μ^+SR measurements were carried out on the M20 surface muon beamline with the LAMPF spectrometer at TRIUMF, the Canada's National Laboratory for Particle and Nuclear Physics located in Vancouver, Canada, which provides a highly intense, polarized beam of positive muons. The samples, 13 polycrystalline disks with 6 mm diameter and 5 mm thickness of NCVO, were mounted on the sample holder for the muon veto cryostat insert[16] by Mylar tape.

Weak transverse-field μ^+SR(wTF-μ^+SR) and zero-field μ^+SR(ZF-μ^+SR) spectra were measured in a nonspin-rotated mode, i.e., the initial muon-spin direction is antiparallel to the muon momentum direction. Here, "weak" means that the applied field is significantly less than any possible spontaneous internal fields ($H_{\rm int}$) in the ordered state. A wTF-μ^+SR technique is sensitive to local magnetic order through the μ^+ spin polarization amplitude. In contrast, ZF-μ^+SR is a sensitive probe of local magnetic (dis)order through the precession of the muon due to internal magnetic fields at the muon interstitial sites.

III. RESULTS

In the inset of Fig. 1(b) we show the typical wTF asymmetry ($A_{\rm TF}$) represented here by the x=0.41 sample at two temperatures, above and below $T_{\rm N}$. In the paramagnetic state, at high temperatures ($T>80$ K), the muon-spin precess at the frequency corresponding to the external transverse field $H_{\rm TF}$=50 Oe. Below $T_{\rm N}$, $A_{\rm TF}$ decreases, due to the strong static internal magnetic fields, $H_{\rm int}$, obeying $H_{\rm int}>H_{\rm TF}$. The remaining oscillating amplitude, shown in the figure, reflects the portion of muons not coupled to $H_{\rm int}$, thus the fraction of the wTF oscillatory signal below $T_{\rm N}$ is negligibly small for the magnetic nature of these compounds. The wTF spectrum is well described by an exponentially relaxing cosine oscillation,

$$A_0 P_{\rm TF}(t) = A_{\rm TF} \exp[-(\lambda_{\rm TF} t)]\cos(\omega_{\rm TF} t + \phi), \qquad (1)$$

where $\omega_{\rm TF}=\gamma_\mu H_{\rm TF}$ with $\gamma_\mu/(2\pi)=13.554$ kHz/Oe. The fit is represented by the solid lines in the inset of Fig. 1(b).

Figure 1(a) depicts the temperature dependence of the normalized $A_{\rm TF}$, $NA_{\rm TF}$, which is proportional to the fraction of the paramagnetic regions in the sample. In NCVO, we find two distinct AF phases; one occurs as Na concentration increases up to $x\sim0.8$ and the transition temperature, $T_{\rm N}$ decreases, the second occurs with $x\geq0.833$, as the Na concentration increases $T_{\rm N}$ takes a sharp turn and increases to higher and higher temperatures with increasing x above 100 K. These observations are summarized in Fig. 1(b) which plots $T_{\rm N}$ versus the Na concentration x. $T_{\rm N}$ is found at the middle of the transition and the errors on $T_{\rm N}$ are taken as 10% of the transition temperature width. Since the $0.083\leq x\leq0.33$ and x=0.775 samples do not experience a sharp magnetic transition, we find these samples to be a mixture of phases. Additionally, we can indicate that a critical doping level $x_{\rm cr}\sim0.83$ separates the two phases. However, we wish to emphasize that both bulk magnetization measurements and x-ray diffraction analysis show that each of these samples is almost a single phase with an orthorhombic structure.[4,13] This clearly indicates the importance of the current microscopic measurements, which show results quite different from the macroscopic bulk measurements.

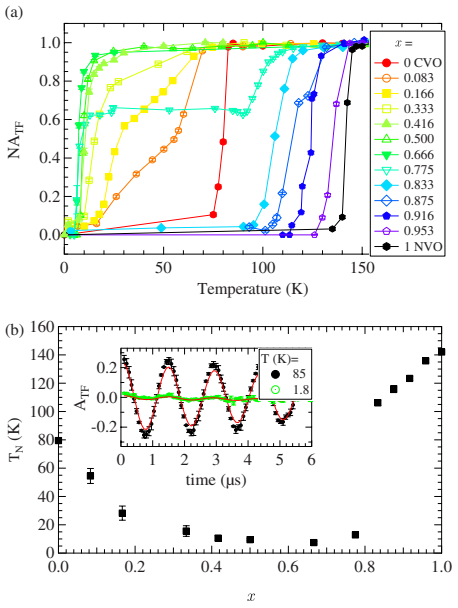

FIG. 1. (Color online) (a) Temperature dependence of the normalized TF asymmetry, $NA_{\rm TF}$, for the complete x family. (b) The transition temperature, $T_{\rm N}$ versus the Na concentration, x. Inset, a typical wTF-μ^+SR spectrum of the NCVO samples. Shown here the paramagnetic phase, T=85, and the ordered state T=1.8 K of the x=0.41 sample. The solid lines indicate a fit to Eq. (1).

A. Insulating region; NCVO with $0<x\leq0.775$

We now explore the two AF phases, identified by the wTF-μ^+SR measurements, using the ZF-μ^+SR technique. The ZF-μ^+SR is a sensitive site-based probe of static magnetism, in which the time-dependent muon polarization signal is determined exclusively by the $H_{\rm int}$'s in the sample. We expect that different magnetic phases would cause different $H_{\rm int}$'s, resulting in different muon frequencies. Therefore, following upon the wTF measurements, we performed detailed ZF measurements for the entire x range. In the $0.41\leq x\leq0.66$ range, we concentrate on the low-T behavior, where the AF transition occurs for $T\leq10$ K. In contrast, for the $x\geq0.833$ samples, we examine a broad T range below 150 K.

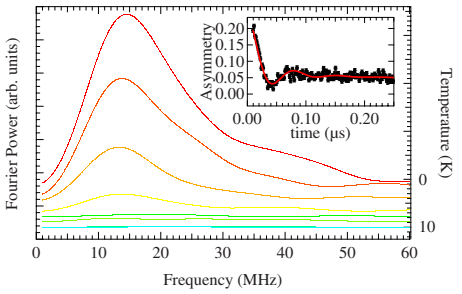

FIG. 2. (Color online) The apodized ZF-μ^+SR FT of the $x=0.41$ sample. Inset shows the time spectrum, the solid line represents a fit to Eq. (3).

Before discussing our current results in NCVO, we briefly summarize the ZF-μ^+SR results of pure CVO.[13] The CVO ZF-μ^+SR spectra indicated four temperature-dependent frequencies below the AF transition, two of which have significant amplitudes. In order to clarify the ground state, dipolar field calculations suggested that AF order exists along the two 1D legs in the zigzag chain, and AF order between the zigzag chains. This result was found to be consistent with neutron measurements both for $H_{\rm int}$'s and the magnitude of the ordered V moment.

The typical raw ZF spectrum, represented by the $x=0.41$ sample, taken at $T=1.8$ K is depict in the inset of Fig. 2. One can clearly see a strongly damped oscillation in the early time domain, $t \leq 0.15$ μs, at the lowest T measured. In order to fit the spectrum, we, at first, attempted to apply a combination of an exponentially relaxing cosine signal and a slowly relaxing signal. The former corresponds to the static AF ordered signal and the latter does to the "1/3" tail for the powder sample,

$$A_0 P_{\rm ZF}(t) = A_{\rm AF} \exp(-\lambda_{\rm AF} t)\cos(\omega_{\rm AF} t + \phi_{\rm AF}) + A_{\rm tail} \exp(-\lambda_{\rm tail} t). \quad (2)$$

Although the ZF spectrum was reasonably fitted by Eq. (2), the initial phase ($\phi_{\rm AF}$) delays by $(66 \pm 2)°$, $(57 \pm 9)°$, and $(44 \pm 6)°$ in the $x=0.41$, 0.5, and 0.66 samples. Since $\phi_{\rm AF}$ should be zero for a simple commensurate AF order, the delay indicates either a wide distribution of $H_{\rm int}$ or a formation of an IC AF order. In fact, the Fourier transform (FT) of the ZF time spectrum in $0.41 \leq x \leq 0.66$ clearly demonstrates the wide field distribution at the muon sites (see the main panel of Fig. 2 as an example of the $x=0.41$ sample). The FT spectrum also indicates the presence of a shoulder on the higher frequency side, suggesting the formation of complex magnetic order. Indeed, the ZF spectrum is better fitted by a zeroth-order Bessel function of the first kind [$J_0(\omega_\mu t)$], especially in explaining the fast relaxing behavior in the early time domain (before 0.02 μs). A ZF spectrum described by J_0 is well-established signature that the μ^+'s experience an IC magnetic field in the lattice.[17] Hence, the ZF-μ^+SR spectra at low T were fitted with a combination of two signals,

$$A_0 P_{\rm ZF}(t) = A_{\rm SDW} \exp(-\lambda_{\rm SDW} t) J_0(\omega_{\rm SDW} t) + A_{\rm tail} \exp(-\lambda_{\rm tail} t). \quad (3)$$

The fit is demonstrated by the solid line in the inset of Fig. 2. In Fig. 3(a), we plot the frequency $f_{\rm SDW} \equiv \omega_{\rm SDW}/2\pi$, extracted from the fits, versus T. For all $x \leq 0.66$, as T increases, $f_{\rm SDW}$ decreases with an increasing slope ($df_{\rm SDW}/dT$) and approaches zero at $T_{\rm N}$. Interestingly, as indicated in Fig. 3(b), the normalized $f_{\rm SDW}$ [$f_{\rm N}=f_{\rm SDW}(T)/f_{\rm SDW}(T \to 0\ {\rm K})$] and the reduced $T(T_{\rm r} \equiv T/T_{\rm N})$ are independent of x [see Fig. 3(b)]. In fact, the $\omega_{\rm N}$ vs $T_{\rm r}$ curves now collapse to a single universal curve, indicating the same origin of the IC transition. This universal curve is well explained by the T dependence of the BCS gap energy, as expected for the order parameter of the IC-AF state.[18,19] This was recently found by a ^{51}V NMR study, which suggested an IC AFM for $x \geq 0.77$.[20] (Note that AF resonance lines in the metallic phase were observed in Ref. 20.) We therefore find that the IC phase in the insulating region includes all compounds, at low T.

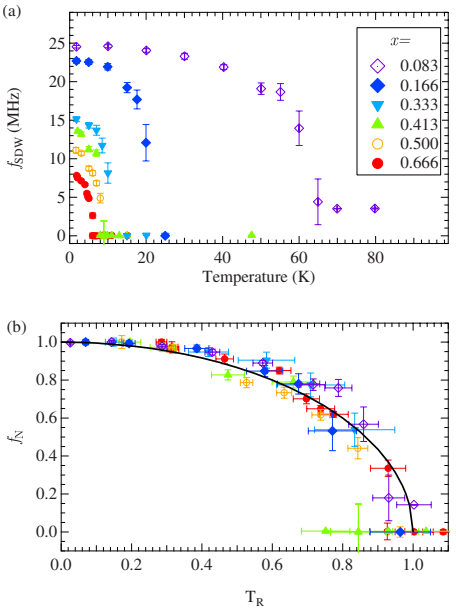

FIG. 3. (Color online) (a) The ZF SDW frequency [$f_{\rm SDW} \equiv \omega_{\rm SDW}/(2\pi)$] versus temperature and (b) the normalized $f_{\rm SDW}$, $f_{\rm N}$, versus the reduced temperature (see text). The solid line indicates the T dependence of the BCS gap energy.

The transverse relaxation rate, $\lambda_{\rm SDW}$, shows typical critical behavior as $T \to T_{\rm N}$, namely, $\lambda_{\rm SDW}$ increases with increasing T up to $T_{\rm N}$ as expected.[21–23] The longitudinal relaxation rate, $\lambda_{\rm tail}$, can, in principle, reveal whether frustration prevents the system from reaching the full static limit, as observed in some highly frustrated systems: normally one expects $\lambda_{\rm tail} \to 0$ (static limit) as $T \to 0$. However, $\lambda_{\rm tail}$ is very small (<1 μs^{-1}) compared with $\lambda_{\rm SDW}$ and difficult to determine reliably, especially in the presence of several signals, hence we cannot make a confident statement.

B. Metallic region; NCVO with $x \geq 0.83$

The FT of the whole x range, at $T=2$ K, is presented in Fig. 4. Clearly, the ZF measurements of the metallic compounds, i.e., $x \geq 0.83$ samples, reveal different behavior than those at smaller x. Unlike the insulating compounds, the metallic compounds, display multiple frequencies (two in $x=0.875$ and four in $x \geq 0.9$), forming one frequency at higher T and vanishing above the phase transition (not

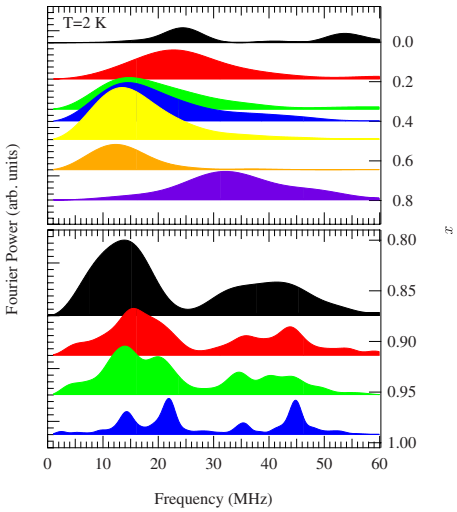

FIG. 4. (Color online) (Color online)The apodized ZF FT of the whole x range, top displays the insulating region characterized by a single wide frequency distribution, bottom shows the metallic region characterized by numerous frequencies.

shown). Therefore, the ZF spectra for these compounds were fitted by a sum of four oscillating signals with a slow exponential relaxation,

$$A_0 P_{\mathrm{ZF}}(t) = \sum_{i=1}^{n} A_i \cos(\omega_i t + \phi_i)\exp(-\lambda_i t) + A_{\mathrm{tail}} \exp(-\lambda_{\mathrm{tail}} t), \tag{4}$$

where $n=4$ and ω_i, ϕ_i, and λ_i are the angular frequency, the initial phase, and the relaxation rate of the ith muon precession, A_{tail} and λ_{tail} are the asymmetry and the relaxation rate for the "1/3 tail" signal,[24,25] as we measured powder samples.

The quality of the fit, shown for NVO, is represented by the solid (green) line in Fig. 6(a). The T dependence of the frequencies, $f_i \equiv \omega_i/(2\pi)$, of the $0.83 \leq x \leq 0.95$ samples shown in Fig. 5(a). In the $x=0.83$ sample, we note that at $T<70$ K two frequencies are distinguished, but at $70 \leq T \leq 110$ K a single frequency is observed. In $x=0.91$ ($x=0.95$), the number of frequencies is decreased from 4, at $T<70$ K to 2 (3) and then to one frequency. Recent neutron-scattering measurements suggests that a small displacement of O^{2-} ions, which leads to a change in the muon sites[14] is the trigger to this intermediate phase. This scenario was also proposed in other compounds.[26] One of the distinctive features in this x range are two common frequencies. At base T, $f_2 \sim 35$ MHz and $f_4 \sim 17$ MHz are x independent. As in the insulating phase, by plotting the frequency versus the reduced temperature results in the collapse of these frequencies to a single curve, suggesting the IC AFM in this phase as well. Figure 5(b) demonstrates this for f_2. In the next section we aim to find the correct spin configuration which produces this behavior.

IV. DISCUSSION

A. Incommensurate AF structure for NVO

We now address the origin of the four frequencies observed in metallic phase using computer simulations. We aim

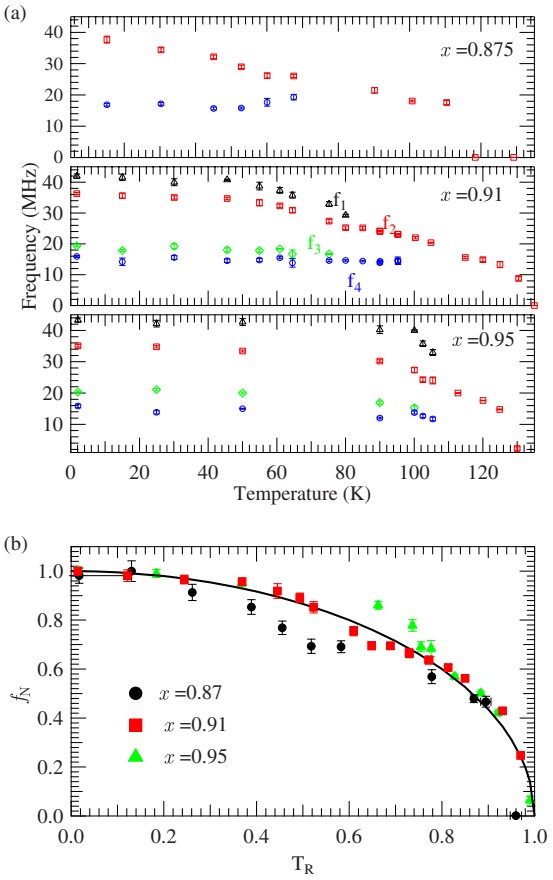

FIG. 5. (Color online) (a) The temperature dependence of the frequencies in the metallic phase, top to bottom, $x=0.875$, 0.91, and 0.95. (b) The reduced-temperature (T_r) dependence of the normalized f_2 frequency, f_N. The solid line demonstrates the BCS gap energy.

to fit the raw experimental data with a minimal number of free parameters. We use the known crystallographic structure in order to create the simulated crystal model.[15] We then find all possible muon sites in the sample using electrostatic potential calculations.[27] Indeed the model finds four distinct muon sites, which was also seen previously in the pure NVO.[13] The next step was to find the correct spin configuration which results in the fields which give the muon precession measured in each site. Hence, dipolar fields were calculated with different independent alignments of the AF moments of the two zigzag chains, residing in the $\widehat{ac}$ plane. The simulation also probed different IC helical modulations, that is the magnetic moment size at the lth unit cell is

$$= m_0 \cos(2\pi k \cdot l), \tag{5}$$

where k is the propagation vector along $\hat{b}$ and m_0 is the V moment size, which is the only free parameter, and is given in Refs. 13 and 14. We average over degenerate states obtained by the simulation in order to accurately describe this model. We use χ^2 criteria as a crude guide in selecting the potential realized state. For comparison, we also performed the same calculation for a linear IC spin-density wave, which is proposed by neutron measurements.[14] However, as seen in

TABLE I. The helical simulation result showing the modulation length along $\hat{b}$, l, and the goodness of fit, χ^2 for Na-concentrations x.

	x	$k[\hat{b}]$ (Å^{-1})	χ^2
Helical	0.916	0.381	1.591
	0.958	0.363	3.732
	1	0.191	0.910
Linear	1	0.571	105.203

Table I, χ^2 for a linear IC-SDW model was always higher than a helical-modulated setup. Figure 6(a) displays the experimental ZF spectrum of NVO taken at $T=2$ K with the simulated spectrum assuming both the helical and linear configuration.

We find that the best fit to the experimental data is, thus, a configuration with an helical IC modulation along $\hat{b}$ axis. Table I summarizes the simulation results and shows the propagation vector k versus x and the χ^2 goodness of fit to the $T=2$ K experimental data of these compounds. The value of NVO is found to be very consistent with that obtained by the recent neutron experiment,[14] namely, the modulation period is $5.214\times b$ along the b axis. However, the powder neutron diffraction result does not suggest a helical IC order but rather a linear IC-SDW order in NVO. The reason for this discrepancy is not clear. We speculate that the since the neutron result was obtained from powder samples through the Rietveld analyses, and the result published may be that of a local minima. Second, it might be that the dipolar field alone, which does not take into account crystal fields might not be fully appropriate to describe such a subtle magnetic state. In fact, a helical IC ordered state is more reasonable in explaining the coexistence of the AF order and metallic conductivity below T_N for NVO. Hence, μ^+SR is found to play a significant role to determine the AF structure in NCVO. In Fig. 6(b), we plot the corresponding magnetic structure suggested by the μ^+SR simulation.

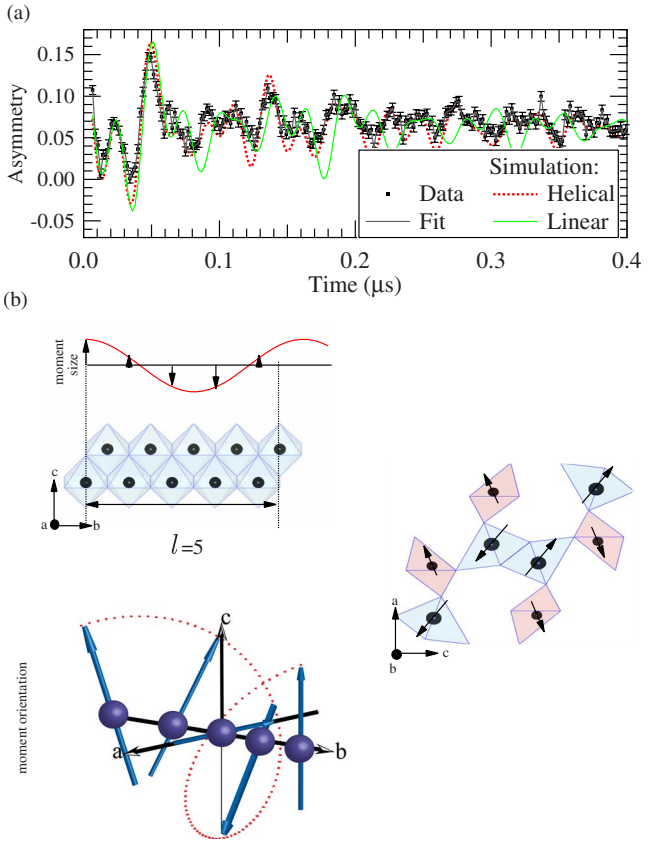

FIG. 6. (Color online) (a) The raw ZF-μ^+SR data of NaV_2O_4. The solid (gray) line indicate a fit, the helical simulation is represented by the dotted line (red), and the linear by the dashed (green) line. (b) The suggested magnetic structure, the moment orientation in the $\widehat{ac}$ plane (right), the moment size and the helical modulation length l (center), the magnetic V ions and their moments in $l=1$.

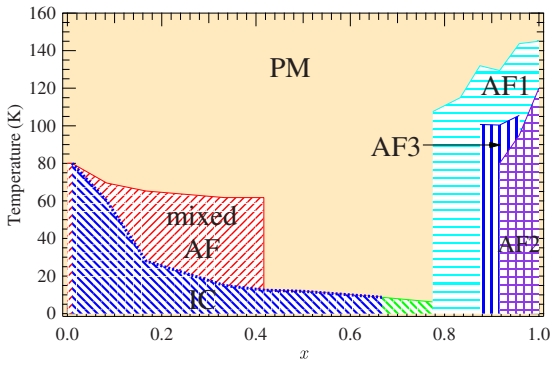

FIG. 7. (Color online) The phase diagram of $Na_xCa_{1-x}V_2O_4$ family. PM: paramagnetic, AF: antiferromagnetic, and IC: incommensurate.

B. Phase diagram

To summarize the μSR measurements of NCVO carried out in the present work, we propose in Fig. 7 the complete phase diagram as a function of x. In particular, the IC-AF phase with its wide field distribution, is present at low temperature of $0<x\leq 0.66$. Interestingly, (above the IC phase), the compounds $0<x\leq 0.41$ show a mixture of CVO and the $x=0.416$ compound by the TF measurements (shown as mixed AF in Fig. 7), but such mixture behavior is absent in the ZF data, in which only the IC phase is identified. The metallic phase, $x\geq 0.83$, is characterized by numerous AF phases. AF1 indicates the AF order identified by a single frequency, found below T_N for $x=0.83$ and at higher temperatures for $x\geq 0.875$. AF2 and AF3 describes the low-temperature AF order characterized by four frequencies occurring in the $x\geq 0.91$. We therefore updated the previously published phase diagram[13] with the introduction of $x=0.41$, identified the IC phase at $x\leq 0.66$, as well as the data on $x=0.875, 0.958$ shed additional light on the multiple AF phases.

V. SUMMARY

In summary, μSR measurements on the $Na_xCa_{1-x}V_2O_4$ family reveal a diverse number of magnetic phases for dif-

ferent x. Compounds in the insulating phase, $0<x<0.8$, indicate a single muon site, data analyses identifies an incommensurate spin-density wave phase. Whereas in the metallic phase, at high Na concentrations, $x>0.8$, data suggests several muon sites. Numerical simulations verify four magnetically distinct muon sites, and validates the existence of an incommensurate helical spin density of the V zigzag chain, with a spin-wave propagation vector **k** along $\hat{b}$ axis. Finally, we wish to point out that, although μ^+SR is usually thought to be incapable to determine the correlation length of the magnetic order, the present study clearly demonstrates that μ^+SR plays a crucial role for clarifying the magnetic structure of NCVO.

ACKNOWLEDGMENTS

We thank the staff of TRIUMF for help with the μ^+SR experiments. Y.I. and J.S. are partially supported by the KEK-MSL Inter-University Program for Oversea Muon Facilities, and J.H.B. is supported at UBC by NSERC of Canada, and (through TRIUMF) by NRC of Canada, K.H.C. by NSERC of Canada and (through TRIUMF) by NRC of Canada, and H.S. by Funding Program for World-Leading Innovative R&D on Science and Technology (FIRST Program) from the Japan Society for the Promotion of Science (JSPS) and Grant-in-Aid for Scientific Research (A), 22246083, JSPS.

*oren@triumf.ca

†Present address: Muon Science Laboratory, Institute of Materials Structure Science, KEK, 1-1 Oho, Tsukuba, Ibaraki 305-0801, Japan.

[1] T. Hikihara, L. Kecke, T. Momoi, and A. Furusaki, Phys. Rev. B **78**, 144404 (2008).

[2] A. A. Zvyagin and S.-L. Drechsler, Phys. Rev. B **78**, 014429 (2008).

[3] O. Tchernyshyov, Phys. Rev. Lett. **93**, 157206 (2004).

[4] T. Varga, J. F. Mitchell, K. Yamaura, D. G. Mandrus, and J. Wang, Solid State Sci. **11**, 694 (2009).

[5] J. Akimoto, J. Awaka, N. Kijima, Y. Takahashi, Y. Maruta, K. Tokiwa, and T. Watanabe, J. Solid State Chem. **179**, 169 (2006).

[6] K. Yamaura, Q. Huang, L. Zhang, K. Takada, Y. Baba, T. Nagai, Y. Matsui, K. Kosuda, and E. Takayama-Muromachi, J. Am. Chem. Soc. **128**, 9448 (2006).

[7] T. Yamauchi, Y. Ueda, and N. Mori, Phys. Rev. Lett. **89**, 057002 (2002).

[8] M. Nakamura, A. Sekiyama, H. Namatame, A. Fujimori, H. Yoshihara, T. Ohtani, A. Misu, and M. Takano, Phys. Rev. B **49**, 16191 (1994).

[9] Z. Q. Mao, T. He, M. M. Rosario, K. D. Nelson, D. Okuno, B. Ueland, I. G. Deac, P. Schiffer, Y. Liu, and R. J. Cava, Phys. Rev. Lett. **90**, 186601 (2003).

[10] K. Yamaura, M. Arai, A. Sato, A. B. Karki, D. P. Young, R. Movshovich, S. Okamoto, D. Mandrus, and E. Takayama-Muromachi, Phys. Rev. Lett. **99**, 196601 (2007).

[11] O. Pieper, B. Lake, A. Daoud-Aladine, M. Reehuis, K. Prokeš, B. Klemke, K. Kiefer, J. Q. Yan, A. Niazi, D. C. Johnston, and A. Honecker, Phys. Rev. B **79**, 180409(R) (2009).

[12] Z. Zhang, D. Louca, A. Visinoiu, S.-H. Lee, J. D. Thompson, T. Proffen, A. Llobet, Y. Qiu, S. Park, and Y. Ueda, Phys. Rev. B **74**, 014108 (2006).

[13] J. Sugiyama, Y. Ikedo, T. Goko, E. J. Ansaldo, J. H. Brewer, P. L. Russo, K. H. Chow, and H. Sakurai, Phys. Rev. B **78**, 224406 (2008).

[14] Hiroshi Nozaki, Jun Sugiyama, Martin Månsson, Masashi Harada, Vladimir Pomjakushin, Vadim Sikolenko, Antonio Cervellino, Bertrand Roessli, and Hiroya Sakurai, Phys. Rev. B **81**, 100410(R) (2010).

[15] H. Sakurai, Phys. Rev. B **78**, 094410 (2008).

[16] http://musr.ca/equip/hold/mvhold.html

[17] J. Major, J. Mundy, M. Schmolz, A. Seeger, K.-P. Döring, K. Fürderer, M. Gladisch, D. Herlach, and G. Majer, Hyperfine Interact. **31**, 259 (1986); A. Amato, R. Feyerherm, F. N. Gygax, A. Schenck, H. v. Löhneysen, and H. G. Schlager, Phys. Rev. B **52**, 54 (1995); N. Papinutto, M. J. Graf, P. Carretta, A. Rigamonti, and M. Giovannini, Physica B **359-361**, 89 (2005).

[18] G. Grüner, *Density Waves in Solids* (Addison-Wesley-Longmans, Reading, 1994), Chap. 4, and references cited therein.

[19] L. P. Le, G. M. Luke, B. J. Sternlieb, W. D. Wu, Y. J. Uemura, J. H. Brewer, T. M. Riseman, R. V. Upasani, L. Y. Chiang, and P. M. Chaikin, Europhys. Lett. **15**, 547 (1991).

[20] H. Takeda, M. Itoh, and H. Sakurai, J. Phys.: Conf. Ser. **200**, 012200 (2010).

[21] D. H. Ryan, J. M. Cadogan, and J. van Lierop, Phys. Rev. B **61**, 6816 (2000).

[22] Y. J. Uemura, T. Yamazaki, D. R. Harshman, M. Senba, and E. J. Ansaldo, Phys. Rev. B **31**, 546 (1985).

[23] G. M. Kalvius, D. R. Noakes, and O. Hartmann, in *Handbook on the Physics and Chemistry of Rare Earths*, edited by K. A. Gschneidner, Jr., L. Eyring, and G. H. Lander (North-Holland, Amsterdam, 2001), Vol. 32, Chap. 206.

[24] T. Ishida, S. Ohira, T. Ise, K. Nakayama, I. Watanabe, T. Nogami, and K. Nagamine, Chem. Phys. Lett. **330**, 110 (2000).

[25] A. Zorko, M. Pregelj, H. Berger, and D. Arcon, J. Appl. Phys. **107**, 09D906 (2010).

[26] J. Sugiyama, Y. Ikedo, P. L. Russo, H. Nozaki, K. Mukai, D. Andreica, A. Amato, M. Blangero, and C. Delmas, Phys. Rev. B **76**, 104412 (2007).

[27] The unit cell was electostatically mapped using the formal charge states for each of the ions in the unit cell. The result indicates four inequivalent magnetic sites next to O^{-2} suggesting a formation of a μ-O covalent bond.